

# Registration and Analysis of Vascular Images\*

Stephen R. Aylward<sup>1</sup>

Julien Jomier<sup>1</sup>

Sue Weeks<sup>1</sup>

Elizabeth Bullitt<sup>2</sup>

Computer-Aided Diagnosis and Display Lab

Medical Image Display and Analysis Group

<sup>1</sup>Department of Radiology

<sup>2</sup>Department of Surgery

The University of North Carolina at Chapel Hill

## Abstract

We have developed a method for rigidly aligning images of tubes. This paper presents an evaluation of the consistency of that method for three-dimensional images of human vasculature. Vascular images may contain alignment ambiguities, poorly corresponding vascular networks, and non-rigid deformations, yet the Monte Carlo experiments presented in this paper show that our method provides registrations with sub-voxel consistency in less than one minute.

Our registration method builds on the principals of our ridges-and-widths tube modeling work; this registration method operates by aligning models of the tubes in a source image with subsequent target images. The registration method's consistency results from incorporate multi-scale ridge and width measures into the model-image match metric. The method's speed comes from the use of coarse-to-fine registration strategies that are directly enabled by our tube models and the model-image match metric. In this paper we also show that the method's insensitivity to local, non-rigid deformations enables the visualization and quantification of the effects of such deformations.

---

\* Submission to the IJCV special issue for UNC MIDAG

## **I. Introduction**

We have developed a fast and automated method for aligning images of tubular structures. We define tubular structures as multi-dimensional networks of generalized cylinders with smoothly varying widths and with paths that may be tortuous, contain cycles, and branch. In this paper, we present Monte Carlo results that demonstrate the speed and consistency of our registration method when dealing with three-dimensional images of human vasculature.

While the general task of aligning images of tubes is difficult, the specific task of aligning vascular images introduces additional complications including vascular network changes and non-rigid deformations. In this paper we will show that for multiple modalities our method is able to produce registrations with sub-voxel consistency in less than one minute despite these difficulties.

Due in part to its consistency, our rigid-registration method also provides a basis for localizing and quantifying non-rigid deformations in the data, i.e., changes in the number, size, and location of tubes. This paper demonstrates methods for visualizing tube deformations. For medical applications, such quantifications and visualizations can be critical to tracking tumor and lesion changes/movement during and after surgical procedures – vessels are well distributed throughout most organs and therefore capture deformations within organs whereas organ surfaces and anatomic landmarks (traditional registration features) are often poorly correlated with internal deformations.

Additionally, compared to surfaces and landmarks, tubes are defined by integrating over larger image regions and therefore are less sensitive to image noise and are better differentiated from surrounding tissue in, and therefore can be more easily registered across, data from multiple imaging devices. Our tube modeling method and the registration method presented in this paper are not dependent on the underlying data. In this paper we demonstrate the application of these methods to contrast enhanced x-ray computed tomography (CT) data and magnetic resonance angiographic (MRA) data.

### **I.1 Details on tube registration difficulties**

Correspondence and alignment ambiguities are inherent to the general task of automatically registering images of tubes. For example, short tube sections of similar width cannot be differentiated from each other, so establishing correspondence can be problematic. Also, the proper alignment of long tube

sections having similar width and uniform curvature is ambiguous – tubes whose widths are poorly differentiated can only resolve alignment in directions normal to their path, i.e., horizontal tubes can only resolve vertical alignment. The alignment process is further complicated by that fact the space between tubes is usually homogeneous – if tubes only partially overlap, it is difficult for a metric, using local measures, to quantify the manner and magnitude of their displacement.

For vascular images, general tube-alignment issues are compounded by vascular network changes and non-rigid deformations. Because of surgical procedures and image acquisition parameters, the number, lengths, and widths of vessels visible in the images may differ and hence the vascular network will appear to change between images. Also, the images may only partially overlap, so vessel segments completely contained in one image may be absent from or only partially or intermittently contained by the other image – causing the vascular network to appear to change. Even more detrimental to establishing correspondence and performing rigid registration, because of patient movement and surgical procedures, localized groups of vessels within and across organs may undergo non-rigid deformations with respect to location, path, and width.

## **I.2 Method Overview**

We have previously presented and extensively evaluated a multi-scale tubular-object segmentation method that is accurate and effective for modeling tubes in a variety of 3D images [Aylward 1996, 2001a; Bullitt 1999, 2001a]. That segmentation method uses ridge traversal to extract the centerline of a tube and medialness measures to subsequently estimate the radius of the tube along that centerline.

Our registration method operates by aligning models of the tubes in a source image with subsequent target images. This model-image registration method attains its consistency by incorporating the mathematical principals of ridges and medialness into the registration optimization process via the structure of the models generated by our tube segmentation method. The method is fast (under one minute to register two large, 3D volumes on a 500 Mhz Pentium III laptop PC) because tubes are sparse in our images and because coarse-to-fine registration strategies are directly enabled by the form of the models and by the model-image match metric.

The model-image match metric used by our registration method was originally published in the proceedings of the 2001 MICCAI conference [Aylward 2001b]. That paper focused on the subjective analysis of the metric and its parameters. This paper provides the first quantitative analysis of the metric

and presents and evaluates an encompassing registration strategy that exploits the metric’s inherent coarse-to-fine registration capabilities.

In the background section of this paper we highlight several approaches to tubular object segmentation and registration. We then motivate our registration work by presenting two sets of medical data that typify the difficulties associated with vascular image registration: vascular network changes and non-rigid deformations due to patient movement and surgical procedures. In subsequent sections, we summarize our segmentation method, detail our registration method, and then analyze our registration method via Monte Carlo experiments and parameter space visualizations using the medical data that motivated our work. We also illustrate our methods ability to localize and quantify non-rigid deformations present in the data. We conclude with a discussion of enhancements that we are investigating to address specific clinical, vascular-image registration problems.

## **II. Background**

There are three categories of methods for registering data: image-image methods, feature-feature methods, and feature-image methods. Most registration methods fall into the first two categories, e.g., mutual information and iterative closest point methods. Our method is an instance of the third category – our method aligns models of the vessels in a source image directly with a target image to quantify and direct the alignment of the source image with the target image. In this section, we review vessel modeling and image registration methods.

### **II.1. Vessel Modeling Methods**

Vessel modeling is a prominent medical image analysis task. A wide variety of excellent methods have been developed [Aylward 2001a; Frangi 1999; Gao 1996; Gerig 1993; Harris 1999; Keller 1995; Lindeberg 1994; Lorenz 1997; Lorigo 1999; Masutani 1998; McInerney 1999; Park 1998; Reuze 1993; Soler 2000; Wilson 1999; Yim 2000]. There are three basic approaches to vessel extraction: centerline-based modeling, spatial filtering, and voxel labeling.

Centerline extraction is the basis of our approach to vessel modeling. Our method starts from an initial point on or near a vessel and from there performs a multi-scale traversal of the vessel’s centerline. Using that centerline, it subsequently estimates the width of the vessel [Aylward 1996 and 2001a]. This approach is based on the multi-scale “core” extraction methods of Pizer [Fritsch 1995; Pizer 1996], the

ridge extraction methods of Eberly [Eberly 1997], and the multi-scale image feature analysis work of Lindeberg [Lindeberg 1994]. Other groups have developed related techniques. The vessel segmentation work lead by Niessen [Frangi 1999] also uses centerline extraction; it begins with an initial specification of a pair of endpoints from which the connected vessel voxels (defined via thresholds) are used to define a path that is iteratively refined to form a centerline representation; the vessel extent normal to that centerline is then determined. By using a single point to initialize the centerline extraction process and by not depending on thresholds, our method is simpler to automate [Bullitt 2001a]. The accurate representation of a vessel's centerline is critical to our registration method.

Spatial filtering methods for vessel segmentation include anisotropic diffusion [Orkins 1997; Du 1995] matched filtering [Gerig 1993], morphological operations [Harris 1999] and level-set evolution [Lorigo 1999; McInerney 1999; Yim 2000]. Matched filtering has been employed by a number of groups. One interesting instance of matched filtering is the traversal technique developed by Gerig [Gerig 1993; Keller 1995] that uses steerable filters. A novel level-set method was developed by Lorigo [Lorigo 1999]. It uses 2<sup>nd</sup>-order level-set information to rapidly extract entire vascular trees. Most spatial filtering methods can be adapted to directly produce centerline estimates.

Statistical pattern recognition approaches to vessel segmentation are numerous [Gao 1996; Park 1998; Soler 2000; Wilson 1999]. One well-developed method [Wilson 1999] uses spatially-adaptive histogram modeling for voxel labeling. That method has demonstrated clinical utility for aneurysm treatment planning. To generate centerline models, the outputs of such voxel-based methods require skeletonization. The accuracy of such centerlines would depend on the skeletonization process employed, e.g., only voxel-level resolution of centerlines is possible via binary morphological erosion.

## **II.2. Registration Methods**

An excellent overview of medical image registration methods is published in [Hill 2001]. The taxonomy presented below differs so as to provide a more intuitive differentiation of our method.

Image-Image registration methods such as mutual-information optimization methods are favored for registering tissue images. These methods, however, are not well suited for registering vascular images. The sparseness of tubes in most vascular images prohibits the use of sampling to speed the calculation of mutual information and other voxel-matching metrics [Collignon 1995; Viola 1995]. These methods are

also poorly suited to handling the alignment ambiguities of tubes and the vascular network changes and non-rigid deformations of vascular images.

Feature-feature registration methods have been heavily investigated for tissue images and several such methods have been developed for vascular images. This class of methods includes iterative closest point [Besl 1992; Ge 1996] and landmark-based techniques [Dryden 1998]. This class also includes 2D/3D registration methods that attempt to determine how to project vessel centers from a 3D image so as to best match the vessel centers in a 2D image formed via X-ray projection through the same anatomy [Bullitt 1999]. Recently, a 3D/3D feature-based registration technique was published [Porter 2001] that uses closest-point pairings of the brightest (by threshold) voxels in MRA and Doppler 3D-US data to quantify their alignment. This method is reported to rigidly register these data in 5-10 minutes and handle initial misalignments of 5-10 degrees. Other groups have also developed MR/3D-US registration methods, but they have focused on image-image matching of vascular structures [Roche 2000].

Feature-feature alignment methods, however, are limited by the speed and accuracy of the feature extraction process. There is often a strong inverse correlation between feature extraction speed and accuracy, and extraction errors in each image may combine to degrade registration accuracy.

Additionally, it is common to reduce feature-feature alignment to point-point alignment and then the mathematical/geometrical characteristics (e.g., orientation and scale) of the underlying structures (e.g., tubes) cannot be exploited during optimization.

Our feature-image registration method only requires the extraction of features (i.e., tubes) from one of the images (e.g., the pre-operative image). For that image, time can be spent making sure the extractions are accurate. Multiple subsequent images (e.g., intra-operative images) can be aligned with those features without additional extractions.

There are relatively few other feature-image registration methods. Some of the hierarchical registration work of Petra van den Elsen falls into this category [van den Elsen 1993]. There has also been research into fitting generic models to multiple images from the same patient – most often this is for the purpose of segmentation but how to align those images could also be deduced. However, the inter-patient variability of the vasculature of nearly every organ (except perhaps the coronary arteries) prohibits the development or fitting of generic models. We know of no other registration method that extracts a patient specific model of the vasculature in one image and aligns that model with subsequent images from that patient.

Three clinical problems motivated our development of this method – those problems and their data are presented in the next section.

### III. Test Data

One of the strengths of our registration method is that it can be applied across imaging modalities. No algorithmic assumptions are made regarding the source or dimensionality of the underlying data. For example, in medicine, it can be used to register CT with MRA data and even pre-operative MRA and CT data with intra-operative 3D-US data. Outside of the medical field, these methods can be applied, for example, to segment rivers and roads in satellite and radar data and to register those data over time despite the creation or destruction of roads, the change in river paths, or significant obscuration.

The work presented in this paper is motivated by three clinical problems: (1) fusing images containing different vascular networks for simultaneous consideration of both networks during surgical planning, (2) tracking vascular network/lesion changes resulting for radiation therapy or surgery, and (3) registering highly detailed pre-operative data with less-detailed intra-operative data for precise surgical guidance. Clinical data representative of the first two problems are detailed below to demonstrate our rigid-registration method’s ability to handle images from different imaging modalities even if those data contain significant vascular networks changes and non-rigid deformations. It is beyond the scope of this paper to address all of the issues surrounding the third clinical problem, intra-operative guidance.

Handling Tube Network Changes (Liver CT Data): An extremely difficult registration problem exists if two images contain multiple tubes, yet only a few of those tubes exist in both images. Such drastic tubular network changes are common to medical data. For example, it would be helpful to fuse medical images acquired at different times after a contrast-agent has been released into the bloodstream to identify areas of rapid contrast uptake (indicative of cancer) or to simultaneously visualize arterial and venous vessels for surgical planning. However, because of contrast flow, the apparent vascular network (type, number, connectivity, and widths) will drastically change between acquisitions. Additionally, because of patient motion such as breathing, there may be non-rigid deformations in the data as well.

Figure 1 illustrates the Live CT data that we used to test the applicability of our method to this class of problems. The first set of CT data (a 256x256x141 voxel volume; 2x2x2mm voxel size) was acquired 30 seconds after contrast agent release; this “portal image” dataset captures the portal-vessel network that carries blood into the liver for filtering. The second set of CT data (256x256x150; 2x2x2mm) was

acquired 60 seconds after the contrast was released, and this “hepatic image” dataset depicts the hepatic-vessel network that carries the filtered blood away from the liver. Our goal is to align the portal with the hepatic data.

The few vessels that are visible in both data must drive the registration process, but these vessels cannot be explicitly differentiated a priori from the rest. Figure 2 illustrates the vessels in these data that can be modeled using our extraction method (Section IV). Additionally, non-rigid deformations exist in these data. Because of the delay between acquisitions, patients move between scans and hold their breath to different depths. The liver moves relatively independently of the surrounding ribs and spinal cord, and the shape of the liver deforms.

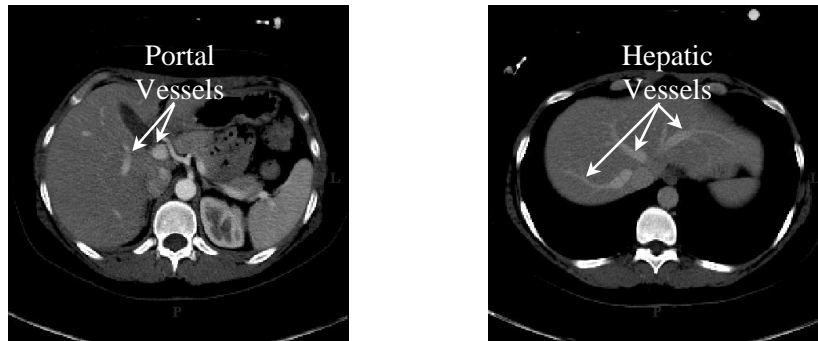


**Figure 1.** *Left: A cross-sectional slice from portal-phase contrast CT data. Slice bisects the liver – the liver is on the left side of the image that corresponds to the right side of the patient. Vessels appear brighter than background because of contrast uptake. Right: A slice from hepatic-phase contrast CT data. Slice is from the top of the liver where the filtered blood is subsequently transported to the heart for re-circulation through the body. These data must be registered so that the vascular networks can be considered together to assess the eligibility of a donor for partial-liver transplantation.*

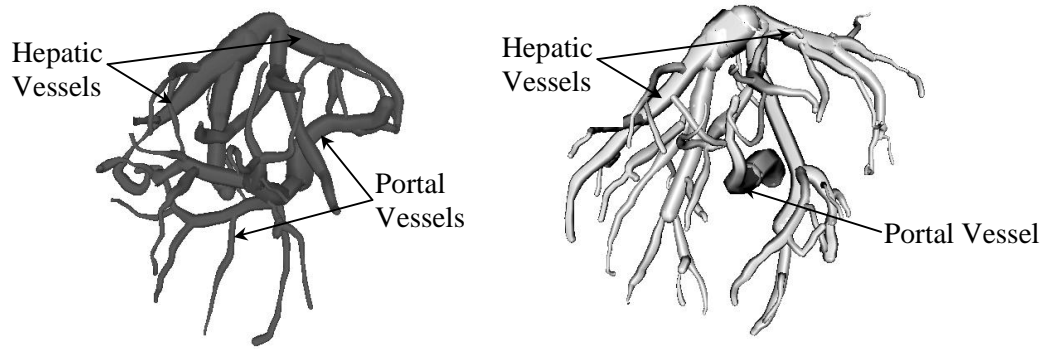


**Figure 2.** *Left: The set of vascular models formed using the portal data (Figure 1-left). Most visible vessels are from the portal venous network, but a few hepatic vessels can also be seen. Right: The set of vascular models formed from the hepatic data (Figure 1-right). The majority of the hepatic vessels can be seen, but only the main portal vessel (central, extending along the point of view) can be seen. Registration is difficult since only a small number of vessels exist in both data and non-rigid deformations are present. The vessel extraction method detailed in Section IV was used to generate these visualizations – manual extraction was performed and required about 15 minutes per dataset.*

Handling Non-Rigid Deformations (Head MRA Data): Localized areas of non-rigid deformation may degrade the consistency with which data can be aligned. In medicine, such local deformations are more the rule than the exception – localized non-rigid deformations may occur naturally by patient breathing or movement as with the Liver CT data presented previously, or the deformations may be induced by treatment such as radiation therapy or even surgery. In medicine and other fields, consistent registration despite local deformations is often important, and applications may often benefit from the quantification of the location and extent of those non-rigid deformations.

Figure 3 shows a sequence of head MRA data from a patient with a successfully treated tumor (an arteriovenous malformation): (1) pre-treatment, (2) post-radiation treatment, and (3) post-surgery. Due to treatment, the number of vessels in the vascular network is reduced and the spatial distribution and size of the vessels about the lesion changes. This lack of correspondence and the non-rigid deformations confound any rigid registration process.



**Figure 3.** Axial maximum-intensity projections of the MRA data of a patient with an arteriovenous malformation (vascular tumor: patient right = image left). Images were taken before pre-treatment, post-radiation treatment, and post-surgery (sequentially – over a 6 month period). Slightly different MRA imaging parameter settings were used to acquire each of these data.

#### IV Vessel Modeling

We have previously presented our vessel segmentation method [Aylward 1996, 2001b]. It is presented again in this paper because its mathematical principals and the form of the model it generates are critical to our registration method.

Our vessel segmentation method operates by performing a multi-scale extraction of the centerline of a vessel and then estimating the width of the vessel about that centerline. Specifically, the method extracts the representation of a vessel in three steps: (1) definition of a seed point on or near a vessel of interest; (2) automatic, multi-scale extraction of an image intensity ridge representing the vessel’s central skeleton; and (3) automatic determination of vessel’s width at each skeleton point.

Step 1: Seed points for initiating the vessel extraction process can be specified manually or determined using application-specific criteria. Manual seed-point ( $\mathbf{x}_0$ ) selection occurs when the user points-and-clicks on a vessel in one slice of a 3D scan and specifies an approximate radius ( $\sigma_0$ ) at that point on the vessel. Automated seed-point selection occurs using local contrast and ridge measures; each voxel in an image (or region of interest) is evaluated to determine if it is sufficiently brighter than its background (to indicate enhancement via contrast) and if it is near the intensity ridge of a tube. An intensity ridge of a tube is defined as a 1D height ridge in 3D:



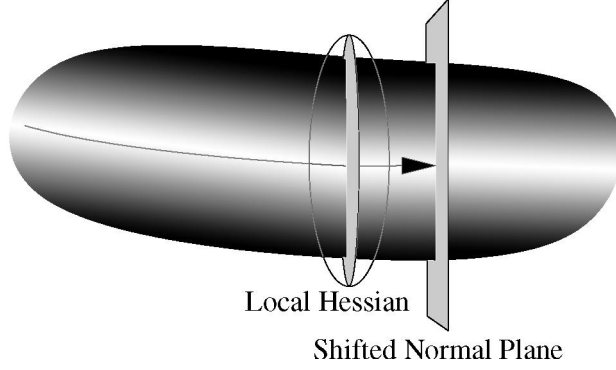


**Figure 4.** Extraction of the central track of a vessel via height ridge traversal. Eigen-vectors of the local Hessian (illustrated as axes of the ellipse) approximate the track’s tangent and normal directions. Traversal occurs by using the shifted approximate normal plane to limit the search for the next ridge point.

Step 3: The central track stabilizes the estimation of the tube’s width. We define the radius at a point  $\mathbf{x}_i$  on a ridge with an initial radius estimate  $r = r_{i-1}$  via

$$r_i = \text{argLocalMax}_r [ M(\mathbf{x}, r) ] \quad (1)$$

where  $M(\mathbf{x}, r)$  is a “medialness” function. Medialness functions respond maximally when applied at the center of a gray-scale object and at a scale ( $r_i$ ) proportional to the width of the object. We have devised a medialness function whose kernel is optimized for the extraction of tubular objects for which the central skeleton has already been extracted. Specifically, to measure medialness at a point  $\mathbf{x}_i$  and a scale  $r$ , we use the weighted-sum of the responses from a series of radially sampled center-on/surround-off medialness kernels,  $K(\mathbf{x}_i, r)$ , applied along and oriented normal to the central skeleton about the point  $\mathbf{x}_i$ .

$$M(\mathbf{x}_i, r) = \sum_{a=-2}^2 d_a K(\mathbf{x}_{i+at}, r) \quad (2)$$

The scalar  $t$  is chosen so as to space the kernels proportionally to the estimated width at the previous point  $r_{i-1}$ . The weights  $d_a$  decrease linearly from  $a = 0$  and sum to one. (**Figure 5**)

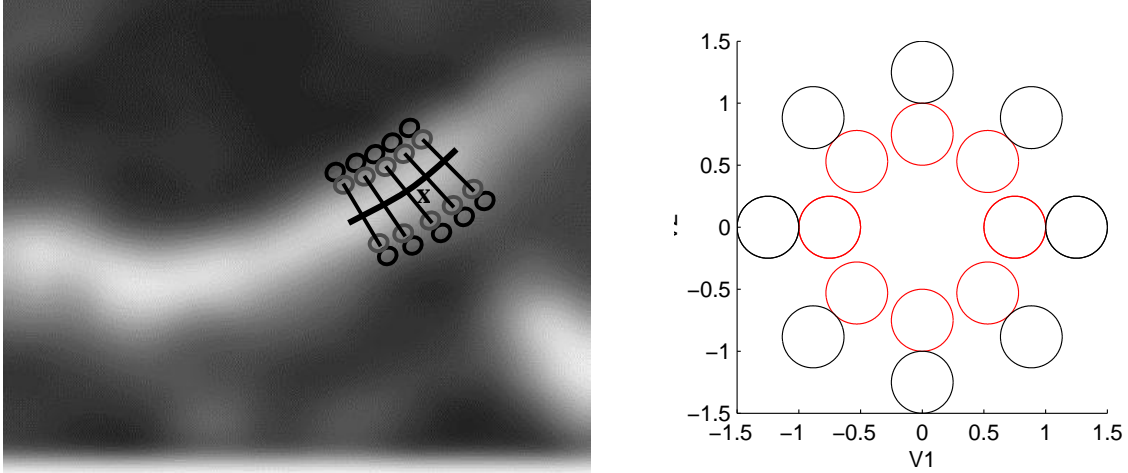


**Figure 5.** (a) A 2D slice along a centerline and passing through the medialness function's kernels: the responses from multiple kernels (aligned along and normal to the centerline) are weighted and summed to estimate the width at a point  $\mathbf{x}$  on the central skeleton. (b) A kernel (seen in 2D cross-section normal to its centerline) of a medialness function is a radial sampling of a center-on (inner circles) / surround-off (outer circles) binary filter of radius  $r$ .

This multi-kernel approach to width estimation exploits the spatial consistency of tubular objects common to medical images. There is significant benefit to this approach. Two of the most important benefits are that the kernels cover a large extent of the tube, thereby providing additional insensitivity to image noise; and the kernels are fit to the spatial curve of the centerline, thereby reducing assumptions about the local shape of the tube.

## V Registering Images of Tubes

Our method is a rigid registration technique. It is formulated as a transformation of point  $\mathbf{x}$  in a source image into the coordinate space  $\mathbf{y}$  of a target image. A rigid transformation occurs as a rotation matrix multiplication plus a translation

$$\mathbf{y} = \mathbf{xR} + \mathbf{o} \quad (3)$$

where

$$\mathbf{R} = \begin{bmatrix} \cos(\alpha)\cos(\beta) & \cos(\alpha)\sin(\beta)\sin(\gamma) - \sin(\alpha)\cos(\gamma) & \cos(\alpha)\sin(\beta)\cos(\gamma) + \sin(\alpha)\sin(\gamma) \\ \sin(\alpha)\cos(\beta) & \sin(\alpha)\sin(\beta)\sin(\gamma) + \cos(\alpha)\cos(\gamma) & \sin(\alpha)\sin(\beta)\cos(\gamma) - \cos(\alpha)\sin(\gamma) \\ -\sin(\beta) & \cos(\beta)\sin(\gamma) & \cos(\beta)\cos(\gamma) \end{bmatrix} \quad (4)$$

is a Euler matrix parameterized by  $\alpha$ ,  $\beta$ ,  $\gamma$  as rotations about the z, y, and x-axes respectively and where

$$\mathbf{o} = [o_x \ o_y \ o_z] \quad (5)$$

## V.1. The Registration Metric

The metric quantifies how well a rotation matrix and offset vector align two vascular images. The metric is based on the fact that vessel centerlines are scaled intensity ridges in the image; therefore, when two vascular images are aligned, the centerline points in one will map to bright points in the other, thereby maximizing our metric, a weighted sum of the scaled intensities of the target image at the transformed points:

$$F(\mathbf{R}, \mathbf{o}) = \frac{1}{\sum_{i=1}^n w_i} \sum_{i=1}^n w_i \mathbf{I}_{\kappa\sigma_i}(\mathbf{x}_i \mathbf{R} + \mathbf{o}) \quad (7)$$

This metric is controlled by the *sampling* of the centerlines ( $\mathbf{x}_i$  and  $n$ ), the *scaling* ( $\kappa\sigma_i =$  standard deviation of the Gaussian kernel used to blur the data) of the image data  $\mathbf{I}$ , and the *weighting*  $w_i$  of the centerline points  $\mathbf{x}_i$ . Via these parameters, coarse-to-fine registration optimization algorithms are possible. A subjective analysis of these parameters is in (Aylward 2001a). A summary is given below. The next section presents the quantitative evaluations of this metric.

*Sampling:* We have performed experiments that show that our method is not sensitive to the number of samples  $n$  if the  $\mathbf{x}_i$  are carefully chosen. For example, to calculate the value of the metric and its derivatives, our optimization strategy only uses one-tenth to one-twentieth of the centerline points extracted during height-ridge traversal. Additionally, the number of samples used is further reduced, and yet the quality of the metric is actually improved, by rejecting any points whose circularity or medialness (see previous section on vessel extraction) is less than 0.2; that is, points are rejected if the local vessel's cross-section has an orientation bias or are poorly differentiated from the background. As expected, if additional points are used, the accuracy of the metric will increase along with the computation time. Based on this trade-off, our optimization strategy increases  $n$  to implement a coarse-to-fine registration heuristic.

*Scaling:* If a tube is differentiated from its background by contrast, an intensity ridge will exist along that tube's center for a range of scales proportional to the radius of the tube. By default (and for all experiment presented in this paper) the local scaling of the image is equal to the radius of the tube ( $\kappa = 1$ ). However, by increasing the scale beyond the radius of the tube (i.e., by using  $\kappa > 1$ ), the intensity ridge will persist

and the spatial range for which that point is the local maximum will increase (barring neighboring objects). See Figure 6. This is another way in which coarse-to-fine registration could be implemented.

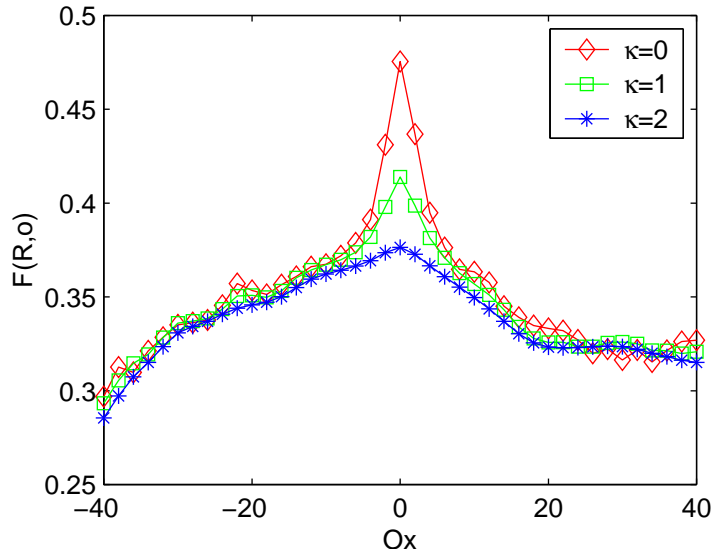


**Figure 6.** Via local image scaling, a larger range of shifting in the  $x$ -axis direction will lead by simple gradient ascent to the ideal  $x$ -offset value of  $o_x=0$ . For  $\kappa=0$ , many local maxima exist. For  $\kappa=2$ , hill-climbing from any  $o_x \in [-40 +20]$  voxels (-50.1mm to +25.0mm) correctly leads to the ideal offset value. Coarse-to-fine registration is possible. This graph used vessels extracted from and applied to the portal liver CT image (Figure 1-left and Figure 2-left).

*Weighting:* As a final technique for smoothing the metric surface, the sample points are weighted based on their radius. The vessel extraction system is capable of capturing vessels whose radius is near the inner scale of the data. While effective for understanding the vascular anatomy, the points on these vessels exist at such a relatively small scale that they have small capture radius and are affected by image noise. We therefore demote the contribution of these points. The weight function is defined to increase exponentially from  $w = 0$  at  $r = 0$  to an asymptote of  $w \cong 1$  at  $r \cong 3$ .

$$w_i = \frac{2}{1 + e^{-2r_i}} - 1 \quad (8)$$

Again, a coarse-to-fine registration strategy could be implemented by equalizing the weighting during optimization to increase the contribution of smaller vessels when in the vicinity of the local maximum.

## V.2. The Registration Metric's Derivative with Respect to Euler's Registration Parameters

The straightforward derivation of the metric to provide transformation parameter gradients to the optimizer would use the rotation and offset components of the Jacobian of the transformation  $J(\mathbf{R}, \mathbf{o})$  and the weighted sum of the scaled gradients in the target image:

$$F(\mathbf{R}, \mathbf{o})d(\mathbf{R}, \mathbf{o}) = \frac{1}{\sum_{i=1}^n w_i} \sum_{i=1}^n w_i J(\mathbf{R}, \mathbf{o}) \nabla \mathbf{I}_{\kappa\sigma_i}(\mathbf{x}_i \mathbf{R} + \mathbf{o}) \quad (9)$$

This approach, however, does not exploit the fact that the  $\mathbf{x}_i$ 's exist on the centerlines tubes. Because of intensity irregularities along a centerline, these derivatives may induce shifts along a vessel whereas ideally shifts will only be produced across a vessel, e.g., horizontal tubes will be limited to inducing vertical shifts. To implement this, at each centerline point, the gradient's influence is limited to the direction normal to the tube in the original data:

Define the normal-plane at a point  $\mathbf{x}_i$  as the matrix

$$\mathbf{N}_i = (\mathbf{v}_{1i} \mathbf{R}) \circ (\mathbf{v}_{1i} \mathbf{R}) + (\mathbf{v}_{2i} \mathbf{R}) \circ (\mathbf{v}_{2i} \mathbf{R}) \quad (10)$$

in which  $\circ$  is the outer-product operator (vector transforms do not involve the offset).

Then the weighted, normal-plane component of the gradient is

$$\nabla \mathbf{I}(\mathbf{x}_i, \mathbf{R}, \mathbf{o})_{\mathbf{v}} = w_i \nabla \mathbf{I}_{\kappa\sigma_i}(\mathbf{x}_i \mathbf{R} + \mathbf{o}) \mathbf{N}_i \quad (11)$$

Next, adjust for the principal orientation of the tubes in a network so that the transformation parameters gradients do not have an orientation bias (if most tubes are horizontal, the system should not be unduly biased towards vertical transformations). This is done via the bias matrix

$$\mathbf{B} = \sum_{i=1}^n w_i \mathbf{N}_i \quad (12)$$

The bias matrix is used to produce the unbiased, weighted, normal-plane component of the gradient defined as

$$\nabla \mathbf{I}(\mathbf{x}_i, \mathbf{R}, \mathbf{o})_{\mathbf{vB}} = \nabla \mathbf{I}(\mathbf{x}_i, \mathbf{R}, \mathbf{o})_{\mathbf{v}} \mathbf{B}^{-1} \quad (13)$$

Leading to the following expression for the transformation parameter gradients:

$$F(\mathbf{R}, \mathbf{o})d(\mathbf{R}, \mathbf{o}) = \sum_{i=1}^n J(\mathbf{R}, \mathbf{o}) \nabla \mathbf{I}(\mathbf{x}_i, \mathbf{R}, \mathbf{o})_{\mathbf{vB}} \quad (14)$$

Since we are only concerned with rigid transformations, we explicitly solve for  $d\mathbf{o}$ ,  $d\alpha$ ,  $d\beta$ , and  $d\gamma$ . The rotation gradients are calculated by projecting  $\nabla\mathbf{I}(\mathbf{x}_i, \mathbf{R}, \mathbf{o})_{\text{VB}}$  onto the tangent of the rotation-circle that passes through  $\mathbf{x}_i$ ; the xy-plane component of this projection estimates the gradient of the metric with respect to  $\alpha$ , the xz-plane component for  $\beta$ , and the yz-plane component for  $\gamma$ , see Figure 7.

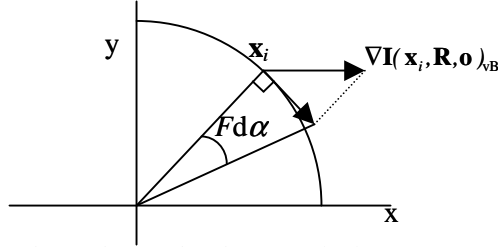


**Figure 7.** Within the xy-plane, the unbiased, weighted, normal-plane component of the image gradient is projected onto the tangent of the rotation-circle passing through  $\mathbf{x}_i$  to determine the gradient of the metric with respect to  $\alpha$ . Similar projections are used within the xz-plane for  $\beta$  and the yz-plane for  $\gamma$ .

### V.3. The Registration Optimization Strategy

Given these metric and metric derivative definitions, a coarse-to-fine gradient ascent registration optimization strategy is possible. The constraints inherent in these measures suggest that gradient ascent should be fast and accurate, and the next section provides parameter-space illustrations and Monte Carlo demonstrations that support our speed and accuracy claims. However, only by defining commensurate offset and rotation units and only by taking advantage of coarse-to-fine methods could an effective method for real-world data be implemented.

In order to be able to efficiently optimize the offset and rotation parameters simultaneously, the spatial and rotation parameters had to be scaled to effect commensurate units. The parameter-space illustrations (and similar illustrations from other datasets) were used to determine these scales. Subjective analyses lead to the selection of 2.5 voxels as an offset unit and 0.1 radians as the rotation unit.

The coarse-to-fine strategy is implemented by increasing the sampling of the tube's centerlines during the two phases of optimization.

Initialization: Euler's registration parameters are set to zero. The metric's only other parameter,  $\kappa$ , is set to one for the entire optimization process presented in this paper.

Phase I: using one twentieth of the centerline points, finite-differences beginning with large (4 unit) and decreasing to small (one unit) step sizes is used to bound the metric’s local maximum.

Phase II: using one tenth of the centerline points, a gradient direction line-search optimization method is used to identify the local maximum within 0.01 units, i.e., within 0.025 voxels and 0.001 radians.

We have also begun investigating the use conjugate gradient and Levenberg-Marquardt optimization techniques that should provide even faster convergence times.

In the next section, using the clinical data, we report the exact numbers of centerline points used, metric and derivative computation times, optimization convergence times (on a 500 Mhz Pentium III laptop PC), and Monte Carlo accuracies.

## **VII. Evaluations**

The two clinical cases demonstrate the application of our method (without modification) to data from different organs and different imaging systems and given vascular network architecture changes and non-rigid deformations. We evaluated our method in three phases: using vessels from the same data to understand our method’s potential given “ideal” correspondence between model and data, using both sets of liver CT data to understand our method’s ability to handle naturally occurring vascular network changes and non-rigid deformations, and using both sets of head MRA data to understand our method’s ability to handle surgery-induced changes in a vascular network and non-rigid image deformations.

We consider a metric and its derivatives to be “effective” for optimizing the parameters of a transformation, if they vary smoothly given small misalignments, if the metric is maximal when the data are aligned, and if the derivatives lead to the alignment of the data for a broad range of misalignments. The visualization of our metric and its derivatives over a range of offsets and rotations provides a means of subjectively assessing these characteristics. The Monte Carlo simulations provide a quantification of the performance of our system to objectively support the presence of these characteristics in our method.

### **VII.1 Effectiveness given rigid mis-registration**

We evaluated our method’s “ideal” performance using the first image, the “portal” image, in the Liver CT sequence to generate visualizations of the metric and its derivatives for a range of offsets and rotations.

Specifically, from the portal data (Figure 1-left), we extracted all of the vessels that could be seen within the liver (Figure 2-left). The extraction process produced 7482 centerline points; the sub-sampling procedure (Section V.1) selected 331 of these points to represent the vessels for registration. Using the same data, we then evaluated the registration metric and its derivatives for a range of x-offsets ( $\pm 20$  voxels = 2.5 cm) and  $\alpha$ -rotations ( $\pm 0.2$  radians = 11.46 degrees in the XY plane). The evaluation of the metric and its derivatives required approximately 0.56 seconds per transformation parameterization. The surface plots of the values are shown in Figure 8.

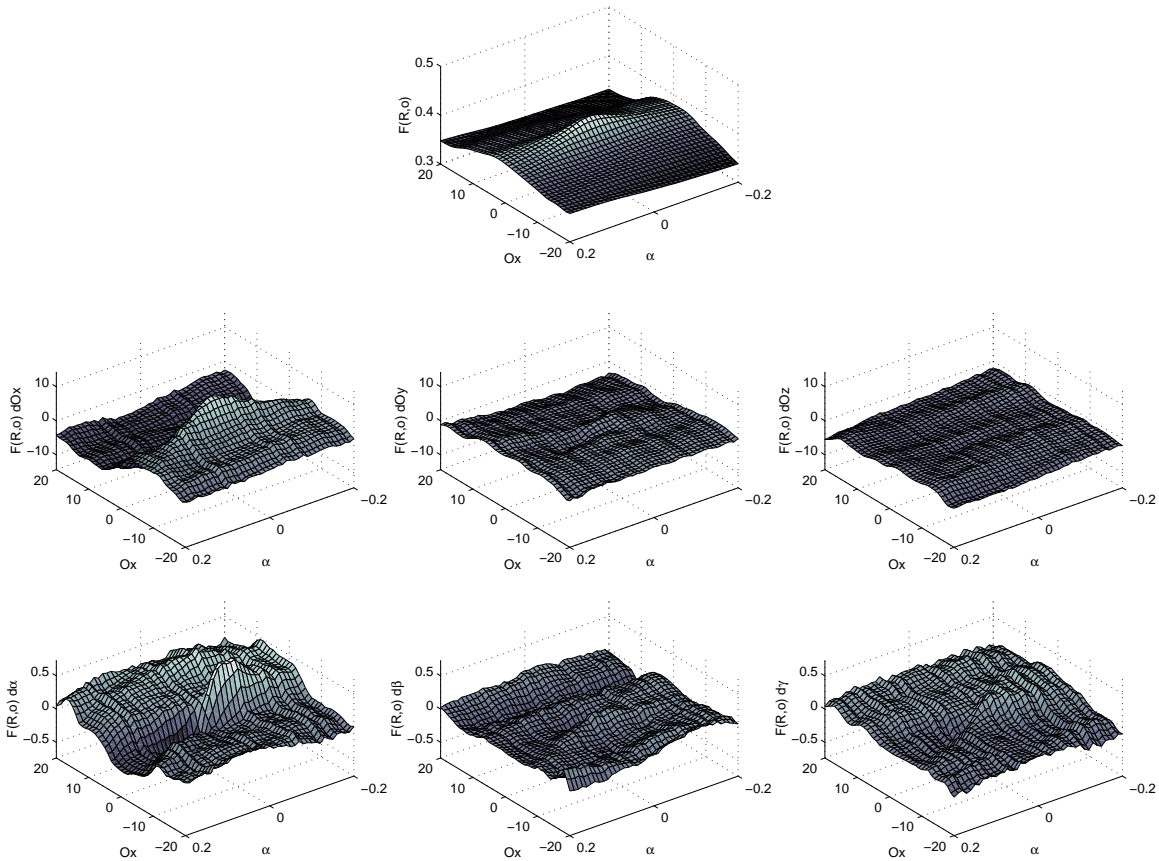


**Figure 8.** The metric and its derivatives evaluated over an x-offset range of  $\pm 20$  voxels (2.5cm) and  $\pm 0.2$  radians (11.46 degrees). Vessels extracted from and applied to the portal image in the Liver CT sequence. Top Row: Metric value. Middle Row: metric derivative in voxels with respect to  $o_x$ ,  $o_y$ ,  $o_z$ . Bottom Row: metric derivative in radians with respect to  $\alpha$ ,  $\beta$ ,  $\gamma$ . The derivatives with respect to  $o_x$  and  $\alpha$  appropriately dominate.

These values do appear to vary smoothly as offset and rotation increases, the metric is maximal given no offset or rotation, and the derivatives lead to the alignment of the data for a broad range offsets and

rotations. All unaffected parameter derivatives remain near zero. However, while  $do_x$  is valid for a wide range of rotations,  $d\alpha$  is only valid if translation has been resolved. These and other observations drove our specification of commensurate offset and rotation units (Section V.3).

As mentioned previously, these visualizations depict the performance of the metric and its derivatives under ideal conditions in which the vessel models were registered with the same data from which they were extracted. Additionally, while these tests excellent for characterizing the metric and its derivatives – these tests are devoid of issues surrounding non-rigid deformations, optimization strategy design, and model architecture inconsistencies (i.e., missing or extraneous vessels in the target image). To test the performance of the entire registration optimization system under the difficult conditions in which these additional sources of error are present, we performed Monte Carlo simulations.

## **VII.2. Monte Carlo Performance – Tube Network Changes**

For the Monte Carlo experiments in this paper we wanted to simulate multiple instances of mis-registration for a pair of images and then measure how well our registration optimization process was able to re-register those images. For this first set of Monte Carlo experiments, we used the portal and hepatic Liver CT data. These images contain significant vascular network changes (Figure 2) and some non-rigid deformations. The apparent lack of correspondence between the features (vessels networks) used for registration makes this a truly difficult registration task.

To maintain realistic conditions, we used the transformation parameters that align these data to center and bound the range of simulated mis-alignments used in the Monte Carlo experiments. The vessel models formed from the portal data (Figure 2-left) were registered with the hepatic data (one slice in Figure 1-right). Registration optimization required 47 seconds. During optimization, 331 points were used to initially bracket the metric maximum, and then 653 points were used to perform gradient-direction line-search to determine the parameters within 0.1 units. The aligned vascular models from both images are illustrated in Figure 9 (only the vessels from the first image, however, were used during registration). The final transformation parameters are given in Table 1. These transformation parameters suggest that Monte Carlo experiments covering a range of  $\pm 10$  voxels and  $\pm 0.1$  radians would represent a realistic range of clinical data acquisition conditions.

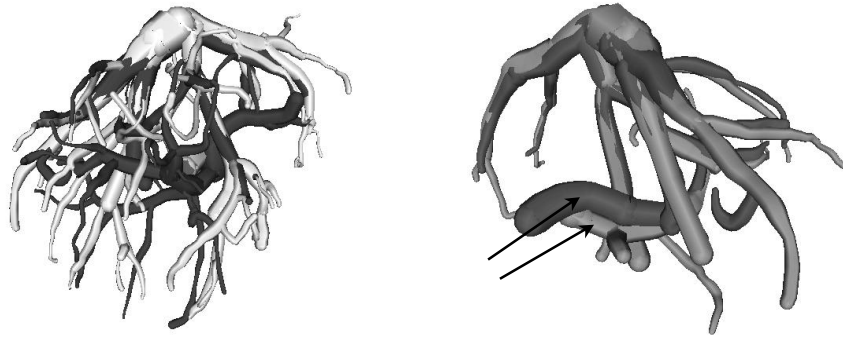


**Figure 9.** Registration of the vessel models first liver CT image with the second liver CT image allows models of all of the portal and hepatic vessel to be viewed simultaneously. Left: All of the vessel models from the two images are shown – vessels from portal Liver CT image in light gray; vessels from hepatic image in dark gray. Right: To illustrate the limited vascular network correspondence and the non-rigid deformations present in the images, the few vessel models that co-exist in both data are shown; the data had undergone non-rigid deformations (arrows), the vascular networks had minimal overlap, the vascular architecture changed, and yet the registration process was effective as indicated by the close correspondence of the surfaces of the models of the same vessels that were formed from the difference images. The sub-selection of vessel models on the right is merely illustrative – it is not part of the registration process.

Parameter	Value (voxels and radians)
$\sigma_x$	0.595
$\sigma_y$	-8.796
$\sigma_z$	0.025
$\alpha$	-0.052
$\beta$	0.037
$\gamma$	-0.030

**Table 1.** Transformation parameters calculated to align the liver’s portal CT data’s vascular models (Figure 9-left) with the liver’s hepatic data (one slice in Figure 1-right).

The Monte Carlo experiments were performed as follows: We generated 100 random transformation parameterizations that mis-aligned the portal-data vascular models with the hepatic data up to  $\pm 10$  voxels ( $\pm 1.25$  cm) and  $\pm 0.1$  radians ( $\pm 5.73$  degrees). From each of these random initial mis-registrations, we then applied our optimization strategy and compared each of the final registration parameters’ values with the mean final registration parameters’ values. Figure 10 plots the relationship between the final offset parameters’ values and the final metric values. Four of the 100 instances converged to local maxima having offsets that were distant from the rest - these instances have low metric values, i.e., the final

registration metric value (Equ. 7) indicates if an optimal final-state has or has not been reached. Table 2 contains a summary of the statistics for the 96 instances that converged to maxima with high metric values.

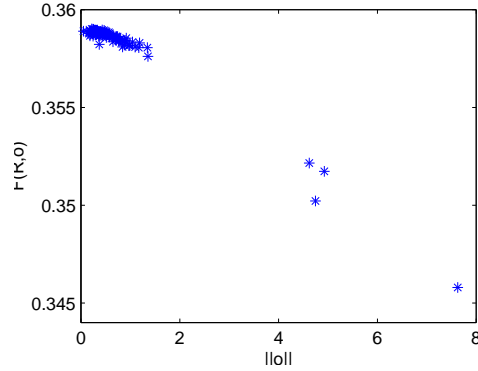


**Figure 10.** A plot showing, for the 100 Monte Carlo registrations, (x-axis) the Euclidean distance from  $\mathbf{o}$  to the average value of  $\mathbf{o}$  –versus- (y-axis) metric value  $F(\mathbf{R}, \mathbf{o})$ . The cluster in the upper left depicts the 96 Monte Carlo registrations that have sub-voxel consistency and high metric values. The four points in the lower right of the plot indicate non-optimal registrations with low metric values. In practice, a heuristic can be implemented to flag and re-optimize registrations that produced poor metric values.

Parameter	Std. Dev. (voxel / radian)	Max difference from mean (vxl/rad)
$\alpha_x$	0.220	0.607
$\alpha_y$	0.400	1.393
$\alpha_z$	0.209	0.615
$\alpha$	0.008	0.024
$\beta$	0.005	0.015
$\gamma$	0.016	0.054

**Table 2.** Results from 96 registrations of the vessel models from the first liver image with the second liver image given random starting points spanning  $\pm 10$  voxel and  $\pm 0.1$  radians. Average offset standard deviations was 0.276 voxel (0.34mm), and average rotation standard deviation was 0.010 radians (0.55 degrees). Four Monte Carlo instances indicated by poor metric values in Figure 10 were not included in these statistics.

The results in Figures 9 and 10 and Table 2 indicate that the registration method is consistent and suggest that it is accurate. The average standard deviation of the final transformation parameters is sub-voxel, sub-millimeter, and within 0.55 degrees. These levels of consistency were achieved despite the fact that

the data had undergone non-rigid deformations, only a few of the vessels modeled in the first image had corresponding vessels in the second image, and multiple additional vessels existed in the second image.

### VII.3. Monte Carlo Performance – Non-Rigid Deformations

The head MRA data shown in Figure 3 challenge rigid vascular image registration methods. We performed two tests: Monte Carlo analysis of the alignment of pre-treatment data with post-radiation data, and visualization of vascular model differences after registration between the pre-treatment and post-surgery data.

Monte Carlo analysis: we followed the same strategy as was used for the liver data. The vascular models from pre-treatment were extracted and aligned with post-radiation data. The resulting transformation parameter values are given in Table 3 and a visualization of the vascular models of the aligned data is shown in Figure 11. This optimization required 39 seconds and used 503 samples during the bounding of the maximum and 993 samples during the localization of the maximum within those bounds. Compared to the registration of the liver data, this registration speed required less time, despite the increase in number of samples, because the average vessel in the AVM data has a significantly smaller scale (radius) than the vessels in the liver data. Hence, the scaled image value and derivative calculations required less time; the time to calculate the metric and its derivative using 993 points from the AVM pre-treatment models requires only 0.17 seconds.

Parameter	Value (voxel / radian)
$\alpha_x$	0.914
$\alpha_y$	-1.876
$\alpha_z$	-3.758
$\alpha$	-0.001
$\beta$	-0.139
$\gamma$	-0.129

**Table 3.** The transformation parameters produced from the use of our method to align the vascular models from AVM pre-treatment (Figure 3 – left) with the post-radiation data (Figure 3 – center). The vascular models also had to be explicitly scaled to match the different voxel sizes of the post-radiation data.

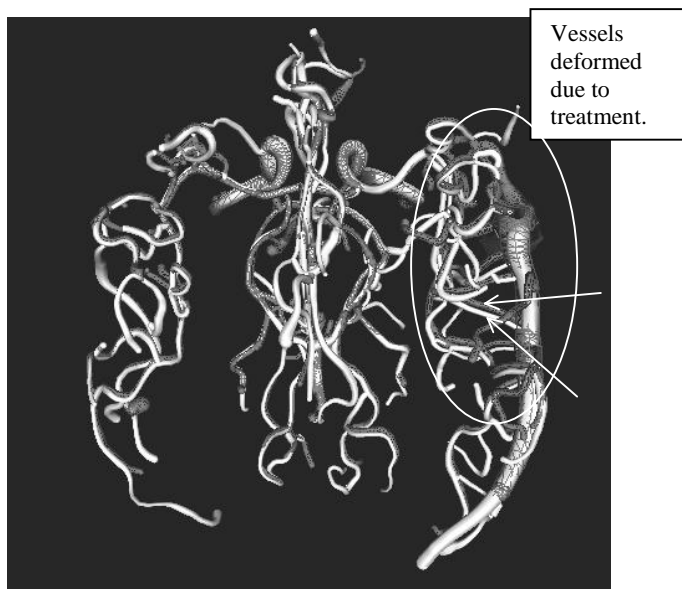


**Figure 11.** Results of alignment of AVM pre-treatment data (used for registration and shown in dark-gray wireframe) with post-radiation (after gamma-knife treatment of the AVM – models not used in registration, but shown as solid light-gray surfaces). The registration parameters are given in Table 2. There is good correspondence between vessels on the patient’s left (image left), but on the right, near the AVM, multiple vessels are misaligned (arrows) and others are missing due to non-rigid deformations that occurred as a result of treatment. Visualizations of such vascular changes helps physicians determine treatment effectiveness.

The Monte Carlo simulations used the same range of random initial starting values as the liver data (offsets of  $\pm 10$  voxels and 0.1 radians). For this set of experiments, three of the one hundred instances failed to converge to a consistent solution (see Figure 12). The statistics from the 97 valid end states are given in Table 3. They indicate that highly consistent results are possible from a wide range of initial mis-registrations despite non-rigid deformations and network architecture changes.

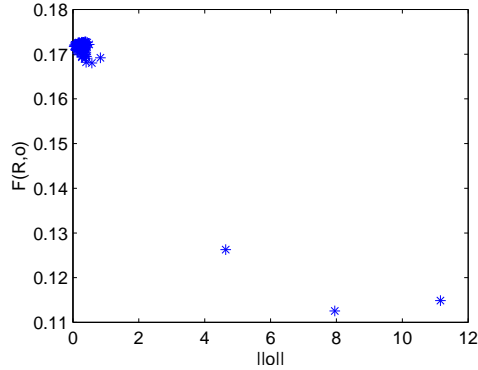


**Figure 12.** A plot showing, for the 100 Monte Carlo registrations, (x-axis) the Euclidean distance from  $\mathbf{o}$  to the average value of  $\mathbf{o}$  –versus– (y-axis) the metric’s value. The cluster in the upper left depicts the 97 Monte Carlo registrations that have sub-voxel consistency and high metric values. The three points in the lower right of the plot indicate non-optimal registrations with low metric values. In practice, a heuristic can implemented to flag and re-optimize image registrations that produced poor metric values.

Parameter	Std. dev. (voxel / radian)	Max difference from mean (vx1/rad)
$o_x$	0.117	0.371
$o_y$	0.109	0.444
$o_z$	0.162	0.518
$\alpha$	0.002	0.006
$\beta$	0.004	0.014
$\gamma$	0.005	0.016

**Table 3.** Statistics from the final states from the registration of pre-treatment and post-radiation head MRA data given initial mis-registrations of up to  $\pm 10$  voxels and  $\pm 0.1$  radians. Average final offset parameter standard deviations was 0.129 voxel (0.16mm), and average final rotation parameter standard deviation was 0.004 radians (0.21 degrees). Three Monte Carlo instances indicated by poor metric values in Figure 12 were not included in these statistics. The parameter values after optimization are consistent even though non-rigid deformations and vascular network architecture changes were present.

As a final illustration of the versatility of the method, we aligned the post-surgery image (Figure 3 - right) with the post-radiation treatment image (Figure 3 - center). All images (and their vessels) were thereby aligned. Illustrations of the vascular changes between the pre-treatment and post-surgery data are given in Figure 13. This visualization displays the distance from the vessel centers in the pre-treatment image to the closest vessel centers in the post-surgery image. This calculation required only a few seconds via the Danielsson distance algorithm. The vessels are shaded to indicate the inter-data vessel distance – bright vessels were strongly affected by radiation and surgery. Other shadings/color-codes can be used to

illustrate how much the vessel radii changed between closest points in these two datasets. We have just begun to investigate and appreciate the clinical utility of these and related visualizations.

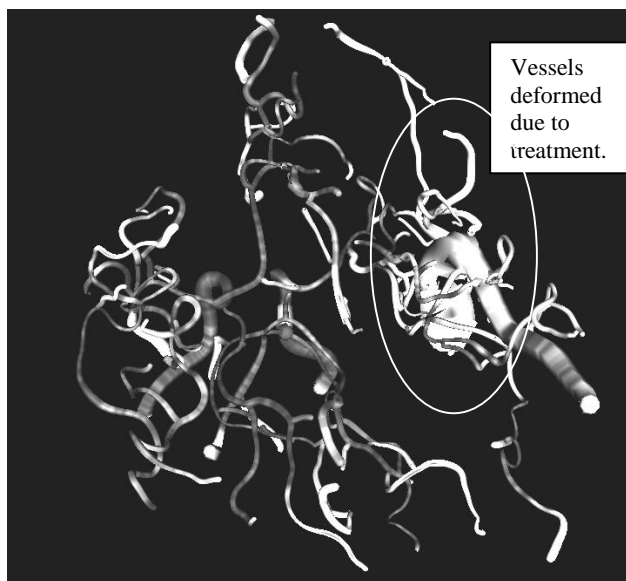


**Figure 13.** A visualization of the effect of radiation and surgery on intracranial vessels containing a tumor (an AVM). Shading encodes the distance from pre-treatment vessels to nearest post-surgery vessels. Ends of some vessels are white because of differences in extraction. Long bright vessels indicate areas of large vascular/anatomic change/shift – the tumor bears the majority of the effects of treatment.

### VIII. Conclusions and Future Work

We have presented a method for registering images of tubes. Monte Carlo experiments and parameter space visualizations presented in this paper indicate that the metric is fast, accurate, and consistent. The method converges in less than one minute and provides extremely consistent (0.1-0.2 voxel and 0.004-0.01 radian standard deviation) registrations of vascular images from different modalities, of different organs, and even if the images contain naturally occurring and surgically induced vascular networks changes and localized non-rigid deformations.

The strength of the system comes from its incorporation of ridge criteria into the model-image match metric and its derivatives. These criteria, for example, limit vertical vessels to affecting horizontal shifts. The metric and its derivatives are also formulated to provide various mechanisms for performing coarse-to-fine registration. The optimization strategy in this paper used the frequency of the sampling of the vessel centerlines to implement a coarse-to-fine registration strategy.

Our work is now focusing on adapting this system to explicitly capture non-rigid tube deformations and smoothly interpolating the deformation of the image data around those tubes. In medicine, the experiments in this paper indicate that such non-rigid deformations are even needed for the accurate alignment of liver portal and hepatic CT images.

The primary application we are developing will exploit our vascular image registration methods for aligning detailed pre-operative images with fast intra-operative images. This will enable the mapping of surgical plans developed pre-operatively onto/into a patient intra-operatively. Surgical procedures will be able to more closely follow surgical plans. This fusion will also enable information (such as tumor margins) to be mapped into the intra-operative data; thereby enabling percutaneous treatment of cancers that are not inherently visible on intra-operative images such as 3D ultrasound.

A WWW site containing additional illustrations of this and related work is at <http://caddlab.rad.unc.edu>. Portions of this work were implemented using the NLM Visible Human Segmentation and Registration Toolkit (The Insight Toolkit: <http://public.kitware.com/Insight/Web/index.htm>). This work was supported in-part by the NIH/NCI R01-CA67812, the NIH/NCI P01-A47982, and an equipment and software grant from Microsoft Corporation. Aspects of this work have been licensed (patent pending) to Medtronic Inc. (Minn., MN) and R2 Technologies (Los Altos, CA).

## IX. References

- [Alperin 1994] N. Alperin, D.N. Levin, C.A. Pelizzari, "Retrospective registration of x-ray angiograms with MR images by using vessels as intrinsic landmarks." *Journal of Magnetic Resonance Imaging* 4: 139-144
- [Aylward 1996] S. Aylward, E. Bullitt, S.M. Pizer, D. Eberly, "Intensity ridge and widths for tubular object segmentation and registration." *IEEE Workshop on Mathematical Methods in Biomedical Image Analysis*, 131-138
- [Aylward 2001a] *Aylward S, Bullitt E, "A Comparison of Methods for Tubular-Object Centerline Extraction," Accepted IEEE Transactions on Medical Imaging, 2001*
- [Aylward 2001b] Aylward S, Weeks S, and Bullitt E, "Analysis of the Parameter Space of a Metric for Registering 3D Vascular Images" *MICCAI 2001*, pages 8
- [Besl 1992] Besl P J and McKay N D "A method for registration of 3-D shapes" *IEEE Trans. Pattern Anal. Mach. Intell.* 14, 1992, pp. 239-56
- [Box 1978] G.E.P. Box, W.G. Hunter, J.S. Hunter, "Statistics for Experiments." *Wiley Series in Probability and Mathematical Statistics*. John Wiley and Sons, New York, NY.
- [Bullitt 1997] E. Bullitt, A. Liu, S. Aylward, and S. Pizer. Reconstruction of the intracerebral vasculature from MRA and a pair of projection views. In *Information Processing in Medical Imaging*, pages 537-542, Poultney, VT, 1997.
- [Bullitt 1999] E. Bullitt, A. Liu, S. Aylward, C. Coffey, J. Stone, S. Mukherji, and S. Pizer. Registration of 3d cerebral vessels with 2d digital angiograms: Clinical evaluation. *Academic Radiology*, 6:539-546, 1999.
- [Bullitt 2001a] Bullitt E, *Aylward S, Bernard E, Gerig G, Special Article. "Computer-assisted visualization of arteriovenous malformations on the home pc." Neurosurgery: 48: 2001, pp. 576-583*

[Bullitt 2001b] Elizabeth Bullitt, Stephen Aylward, Keith Smith, Suresh Mukherji, Michael Jiroutek and Keith Muller, "Symbolic description of intracerebral vessels segmented from magnetic resonance angiograms and evaluation by comparison with X-ray angiograms" *Medical Image Analysis* 5: 157-169, 2001.

[Collignon 1995] Collignon A, Maes F, Delaere D, Vandermeulen D, Suetens P and Marchal G, "Automated multi-modality image registration based on information theory" *Information Processing in Medical Imaging* 1995 ed Y Bizais, C Barillot and R Di Paola (Dordrecht: Kluwer Academic, 1995 pp 263-74

[Du 1995] Y. Du, D. Parker, and W. Davis. Improved vessel visualization in MR angiography by nonlinear anisotropic filtering. *Journal of Magnetic Resonance Imaging*, 5:353-359, 1995.

[Dryden 1998] Dryden I and Mardia K 1998 *Statistical Shape Analysis* (New York: Wiley)

[Eberly 1996] D. Eberly. *Ridges in Image and Data Analysis*, volume 7 of *Computational Imaging and Vision*. Kluwer Academic Publishers, Dordrecht, 1996.

[Frangi 1999] A. F. Frangi, W. J. Niessen, R. M. Hoogeveen, T. Van Walsum, and M. A. Viergever. Model-based quantitation of 3-d magnetic resonance angiographic images. *IEEE Transactions on Medical Imaging*, 18(10):946-956, October 1999.

[Fritsch 1995] D.S. Fritsch, D. Eberly, S.M. Pizer, and M.J. McAuliffe. Stimulated cores and their applications in medical imaging. In Y. Bizais, C. Barillot, and R. DiPaola, editors, *IPMI 1995: Information Processing in Medical Imaging*, pages 385-68. *Kluwer Series in Computational Imaging and Vision*, 1995.

[Gao 1996] L. Gao, D. G. Heath, B. S. W. Kuszyk, and E. K. Fishman. Automatic liver segmentation technique for three-dimensional visualization of CT data. *Radiology*, 201(2):359-364, November 1996.

[Ge 1996] Y Ge, CR Maurer Jr, JM Fitzpatrick. Surface-based 3-D image registration using the Iterative Closest Point algorithm with a closest point transform. *Medical Imaging 1996: Image Processing*, Proc. SPIE, 1996

- [Gerig 1993] G. Gerig, T. Koller, G. Szekely, C. Brechbuhler, and O. Kubler. Symbolic description of 3-d structures applied to cerebral vessel tree obtained from MR angiography volume data. In *Information Processing in Medical Imaging '93: Lecture Notes in Computer Science 687*, pages 94-111, 1993.
- [Harris 1999] K. Haris, S. N. Efstraatiadis, N. Maglaveras, C. Pappas, J. Gourassas, and G. Louridas. Model-based morphological segmentation and labeling of coronary angiograms. *IEEE Transactions on Medical Imaging*, 18(10):1003-1015, October 1999.
- [Hill 2001] D Hill, P Batchelor, M Holden, D Hawkes, "Medical Image Registration" *Phys. Med. Biol.* 46, 2001
- [Hoogeveen 1998] R. M. Hoogeveen, C. J. G. Bakker, and M. A. Viergever. Limits to the accuracy of vessel diameter measurement in MR angiography. *Journal of Magnetic Resonance Imaging*, 8, 1998.
- [Koller 1995] T. Koller, G. Gerig, G Szekely, and D. Dettwiler. Multiscale detection of curvilinear structures in 2-d and 3-d image data. In *Proceedings of the 5th International Conference on Computer Vision*, pages 864-869, Boston, MA, 1995. IEEE Computer Society Press.
- [Lindeberg 1994] Tony Lindeberg, *Scale-Space Theory in Computer Vision*, Kluwer Academic Publishers, Dordrecht, Netherlands, 1994
- [Lorenz 1997] C. Lorenz, I. C. Carlsen, T. M. Buzug, C. Fassnacht, and J. Weese. Multi-scale line segmentation with automatic estimation of width, contrast, and tangential direction in 2d and 3d medical images. In J. Troccaz, E. Grimson, and R. Mosges, editors, *CVRMed-MRCAS '97*, pages 233-242. Springer-Verlag, 1997.
- [Lorigo 1999] L. M. Lorigo, O. Faugeras, W. E. L. Grimson, R. Keriven, R. Kikinis, and C. F. Westin. Co-dimension 2 geodesic active contours for MRA segmentation. In *Information Processing in Medical Imaging '99: Lecture Notes in Computer Science 1613*, pages 126-139, 1999.
- [Masutani 1998] Y. Masutani, T. Schiemann, and K. H. Hohne. Vascular shape segmentation and structure extraction using a shape-based region-growing model. In *Proceedings of Medical Image Computing and Computer-Assisted Intervention, Lecture Notes in Computer Science 1496*, pages 1242-1249, 1998.

[McInerney 1999] T. McInerney and D. Terzopoulos. Topology adaptive deformable surfaces for medical image volume segmentation. *IEEE Transactions on Medical Imaging*, 18(10):840-850, October 1999.

[Morse 1994] B. S. Morse, S. M. Pizer, and D. S. Fritsch. Robust object representation through object-relevant use of scale. In *Medical Imaging '94: Image Processing*, volume 2167, pages 104-115. SPIE, 1994.

[Orkisz 1997] M.M. Orkisz, C. Bresson, I.E. Magnin, O. Champin, and P.C. Douek. Improved vessel visualization in MR angiography by nonlinear anisotropic filtering. *Magnetic Resonance Imaging*, 37, 1997.

[Park 1998] W. Park, E. A. Hoffman, and M. Sonka. Segmentation of intrathoracic airway trees: A fuzzy logic approach. *IEEE Transactions on Medical Imaging*, 17(4):489-497, 1998.

[Pizer 1996] S. M. Pizer, D. Eberly, B. S. Morse, and D. S. Fritsch. Zoom-invariant vision of figural shape: The mathematics of cores. In *Computer Vision and Image Understanding*, 1996.

[Porter 2001] Brian C. Porter, Deborah J. Rubens, John G. Strang, Jason Smith, Saara Totterman, Kevin J. Parker3D, "Registration and Fusion of Ultrasound and MRI Using Major Vessels as Fiducial Markers" *IEEE TMI* 20(4) 2001

[Reuze 1993] P. Reuze, J. L. Coatrieux, L. M. Luo, and J. L. Dillenserger. A 3-d moment based approach for blood vessel detection and quantification in MRA. *Technology and Health Care*, 1:181-188, 1993.

[Roche 2000] A Roche, X Pennec, G. Malandain, N. Ayache, S. Ourselin, "Generalized Correlation Ratio for Rigid Registration of 3D Ultrasound with MR Images" *Rapport de recherche de l'INRIA-Sophia Antipolis*, # 3980, Page 24

[Sato 1997] Y. Sato, S. Nakajima, H. Atsumi, T. Koller, G. Gerig, S. Yoshida, and R. Kikinis. 3d multi-scale line filter for segmentation and visualization of curvilinear structures in medical images. In J. Troccaz, E. Grimson, and R. Mosges, editors, *CVRMed-MRCAS '97*, pages 213-222. Springer-Verlag, 1997.

[Sobol 1994] Llya M. Sobol'. A Primer for the Monte Carlo Method. CRC Press, Boca Raton, 1994.

[Soler 2000] L. Soler, H Delingette, G. Malandain, N. Ayache, C. Koehl, J. M. Clement, O. Dourthe, and J. Marescaux. An automatic virtual patient reconstruction from CT-scans for hepatic surgical planning. In J. D. Weswood, editor, *Medicine Meets Virtual Reality*, pages 316-322. IOS Press, 2000.

[van den Elsen 1994] van den Elsen P A, Maint "Registering images using correlation of geometrical features" *IEEE Trans. Med. Imaging* 14 1994, pp. 384-96

[Wilson 1999] D. L. Wilson and J. A. Noble. An adaptive segmentation algorithm for time-of-flight MRA data. *IEEE Transactions on Medical Imaging*, 18(10):938-945, October 1999.

[Yim 2000] P.J. Yim, P.L. Choyke, and R.M. Summers. Gray-scale skeletonization of small vessels in magnetic resonance angiography. *IEEE Transactions on Medical Imaging*, 19(6):568-576, June 2000.